Available online at www.sciencedirect.com
ScienceDirect
Journal of the European Ceramic Society 31 (2011) 2887–2896
www.elsevier.com/locate/jeurceramsoc

Thermally stable and photocatalytically active titania for ceramic surfaces

M. Hofer, D. Penner *

Laboratory of Ceramic Materials, Institute of Materials and Process Engineering IMPE, Zurich University of Applied Sciences, Technikumstrasse 9, 8400 Winterthur, Switzerland

Received 7 January 2011; received in revised form 21 June 2011; accepted 10 July 2011
Available online 7 August 2011

Abstract

The most photocatalytically active titania modification anatase must be stabilised to achieve high photocatalytic activity in ceramic processes at temperatures above 1000 °C. Thermally stable TiO_2 powders were prepared by the addition of silica and boehmite nanoparticles and deposited on corundum substrates and lead-free glazes. The powders and coatings were fired at increasing temperatures, and stabilisation of the anatase phase was achieved up to 1200 °C. In general, thermal stability was found to be lower when coated on substrates compared to the powder alone, and the extent of reduction depended on the chemical composition of the substrate. Only a slight modification of the titania electronic structure was found, indicating only weak interactions between silica and titania. Based on these results it is possible to assume an amorphous silica and alumina shell encases the titania particles which prevents grain growth and the anatase to rutile phase transformation.

Keywords: TiO_2; SiO_2; Glass; Firing; Phase transformation

1. Introduction

Research on TiO_2 semiconductor photocatalysis in general, and on functional surfaces in particular, has been a subject of great interest in recent decades. TiO_2 is used for disinfection and detoxification of water and wastewater, air purification, anti-fogging surfaces, self-cleaning surfaces, self-sterilizing surfaces, amongst other applications.[1–5] Using TiO_2 oxidation processes in self-sterilizing coatings to disinfect and produce hygienic surfaces is an interesting application for photocatalysis.[6] Regarding the proliferation of infectious diseases by mutated microorganisms in recent years, self-disinfecting surfaces in public areas may be an important development for the future. For example, Kikuchi et al.[7] and Sunada et al.[8] demonstrated the decomposition of *Escherichia coli* on a photocatalytically active titanium dioxide surface on glass substrates. *E. coli*, *Pseudomonas aeruginosa*, *Staphylococus aureus*, *Enterococcus hirae* and *Bacteroides fragilis* were decomposed in suspension by Tsuang et al.[9] Other studies have shown the decomposition of different types of microorganisms such as MS-2 phages,[10] hepatitis B viruses,[11] cancer cells with cell-specific antibody-TiO_2 bioconjugates[12,13] and algae and daphnids.[14] The decomposition of microorganisms on ceramic substrates was also demonstrated by Zan et al.[11,15]

However, because anatase is the most photocatalytically active modification of TiO_2, a key issue for the development of photocatalytically active ceramic surfaces is the anatase (A) to rutile (R) phase transformation.[2,16–18] Usually, nanocrystalline anatase is transformed to rutile in the temperature range from 600 °C to 700 °C.[19] This phase transition prohibits the direct application of nanocrystalline anatase in ceramic processes such as firing or glazing which usually require temperatures between 1000 and 1200 °C. Rego et al.[20] fired screen-printed TiO_2 coatings on glazed ceramic tiles at 850 °C and Marcos et al.[21] found the optimal working temperature range to be from 600 °C to 950 °C to prevent the A–R phase transition and achieve high photocatalytic activity. Bondioli et al.[22] fired a TiO_2-containing sol deposited by air-brushing on unglazed ceramic tiles up to 600 °C for 5 min and Yoo et al.[23] fired a transparent TiO_2 sol on glaze-coated tiles up to 700 °C, also to prevent the A–R phase transition.

To develop hard, abrasion resistant and photocatalytically active titania coatings prepared at temperatures above 1000 °C

* Corresponding author. Tel.: +41 58 934 73 23.
E-mail address: dirk.penner@zhaw.ch (D. Penner).

0955-2219/$ – see front matter © 2011 Elsevier Ltd. All rights reserved.
doi:10.1016/j.jeurceramsoc.2011.07.016

the most photocatalytically active titania modification anatase must be stabilised. The anatase to rutile transformation rate is dependent on dopants, dopant concentration and other compounds present such as oxides. Several studies showed the increase of the transformation rate in the presence of Fe_2O_3,[24,25,27] iron chlorides,[24] NiO,[26] CoO,[26] MnO_2,[26,27] CuO,[26,27] Li_2O,[25] LiF,[27] Li_2CO_3,[27] K_2O and Na_2O.[25,28] Other oxides such as CeO_2,[29,30] Eu and Sm[31] inhibit the A–R phase transition rate. Low-cost oxides alumina and silica increase the thermal phase stability of anatase at high temperature; Ding et al.[32] demonstrated the thermal stabilisation of a sol–gel synthesised anatase powder by a small fraction of alumina, and Yang and Ferreira[33,34] found an inhibitory effect of sol–gel derived alumina and Al_2O_3–SiO_2 powders on the anatase to rutile phase transition. Baiju et al.[35] and Periyat et al.[36] also showed increased thermal stability and photocatalytic activity of sol–gel synthesised mixed TiO_2–SiO_2 and TiO_2–Al_2O_3–SiO_2 powders.

To the extent of our knowledge, the above authors limited their investigations to demonstrating the thermal stability of anatase powders, and there are no reports on the behaviour of stabilised TiO_2 coatings made on substrates. In the present work we show a simple method to prepare thermally stable titania powders and coatings using tetraethyl orthosilicate and pre-formed boehmite and anatase nanoparticles. We demonstrate and discuss the thermal stability of the powders and coatings made on corundum and three different lead-free glazes fired above 1000 °C. Further, we characterise the material using XRD, FT-IR and UV–vis spectroscopy, XPS, SEM-EDS and investigate the photocatalytic activity of the material using methylene blue as the model organic compound.

2. Experimental

2.1. Stabilised titania powder preparation

The synthesis of silica- and boehmite-stabilised titania was performed using tetraethyl orthosilicate (TEOS) as precursor. The molar ratio of TEOS to boehmite (AlOOH) was 3/1. In some experiments the boehmite fraction was replaced completely by TEOS. The mixtures investigated contained 13, 20, 25, 36, 47, 57, 76, 92, 96 and 98 wt% titania, with the total amount of material (TEOS + AlOOH + TiO_2) fixed at 77 mmol. The experiments consisted of the following steps: TEOS (Sigma–Aldrich) was dissolved in 33.3 g anhydrous ethanol, then hydrolised by adding 3.33 g of 0.04 M aqueous hydrochloric acid and stirring at 1000 rpm for 24 h at room temperature. In a separate step, pre-formed titania nanoparticles (40 wt% in water; VP Disp. W 740 X, Evonik) were added and stirred for 18 h at 1000 rpm. The final step involved the addition of boehmite nanoparticles (25 wt% in water; Disperal P2, Sasol) and stirring for 6 h at 1000 rpm. For powder production the dispersions were dried in two stages, 25 °C for 24 h and 80 °C for 1 h, before grinding to a powder. The powders were fired for 30 min at various temperatures between 100 °C and 1400 °C in steps of 100 °C.

2.2. Substrate and titania coating preparation

Fired stoneware substrates were glazed with three different lead-free glaze compositions. Na–K-glaze 1 contained 19% Na_2O, 2% K_2O, 3% CaO, 8% ZnO, 2% Al_2O_3, 66% SiO_2. The glaze was first dried at 25 °C and then at 80 °C for 60 min before firing using a controlled ramp of 100 °C/h to 650 °C, 150 °C/h to 1100 °C and holding for 20 min. Na–B-glaze 2 contained 15% Na_2O, 51% SiO_2, and 34% B_2O_3 and the glaze was dried and fired as per glaze 1. Ca–Ba–B-glaze 3 contained 5.5% CaO, 10.6% Al_2O_3, 56.3% SiO_2, 5.0% BaO, 22.6% B_2O_3. The glaze was dried at 80 °C for 60 min before firing using a ramp of 500 °C/h to 1100 °C and holding for 10 min. The glazed substrates and unglazed corundum substrates were coated with the titania dispersion using a dip-coating process in a separate step. The coated area on the substrates covered 2.5 cm × 4.0 cm and a withdrawal velocity of 300 mm/min for the coating was used. The coatings were dried at room temperature for 1 h and at 80 °C for 1 h and then fired at 1080 °C for various durations from 1 to 30 min.

2.3. Characterisation methods

The phase composition of the powders and coatings was determined by X-ray diffraction (XRD) using a Bruker Advance D8 diffractometer with Cu Kα radiation, a resolution of 0.0057° and 0.5 s/step acquisition time. Quantitative determination of the phase composition, crystallite size and lattice parameters was performed via the Rietveld-Method[37] using BGMN Autoquan software version 2.7 (GE Inspection Technologies GmbH). The weighted profile *R*-factors (R_{wp}) for refinements were below 10%. The electronic structure of the powders was determined by Fourier transform infrared spectroscopy (FT-IR) measurements on a Perkin–Elmer Spectrum 100 spectrometer with a resolution of 4 cm^{-1} and a measurement range from 4000 to 600 cm^{-1}. Reflection ultraviolet–visible spectroscopy (UV–vis) measurements were recorded with a Perkin–Elmer Lambda 950 spectrophotometer with a resolution of 1.0 nm and a range from 300 to 650 nm. Scanning electron microscopy (SEM) and energy dispersive X-ray spectroscopy (EDS) were performed on a Zeiss Supra 40 PV. X-ray photoelectron spectroscopy (XPS) was performed on a SPECS Compact ESCA System SAGE HR 100 spectrometer using Mg Kα radiation.

2.4. Determination of photocatalytic activity

The photocatalytic activity of the stabilised anatase coatings was determined using an aqueous solution of methylene blue (95%, Sigma–Aldrich) at a concentration of 10 μmol/l. An 8 cm diameter borosilicate petri dish was used as the photocatalytic reactor. The light source consisted of an 830 W/m^2 xenon emitter with wavelength range of 300–830 nm to mimic the natural wavelengths and radiation intensity of the sun. The distance between the lamp and the coatings was 21.0 cm. The reactor was cooled by a fan with a flow of 60 m^3/h and 20–25 °C air temperature. UV–vis spectroscopy to measure the absorption of

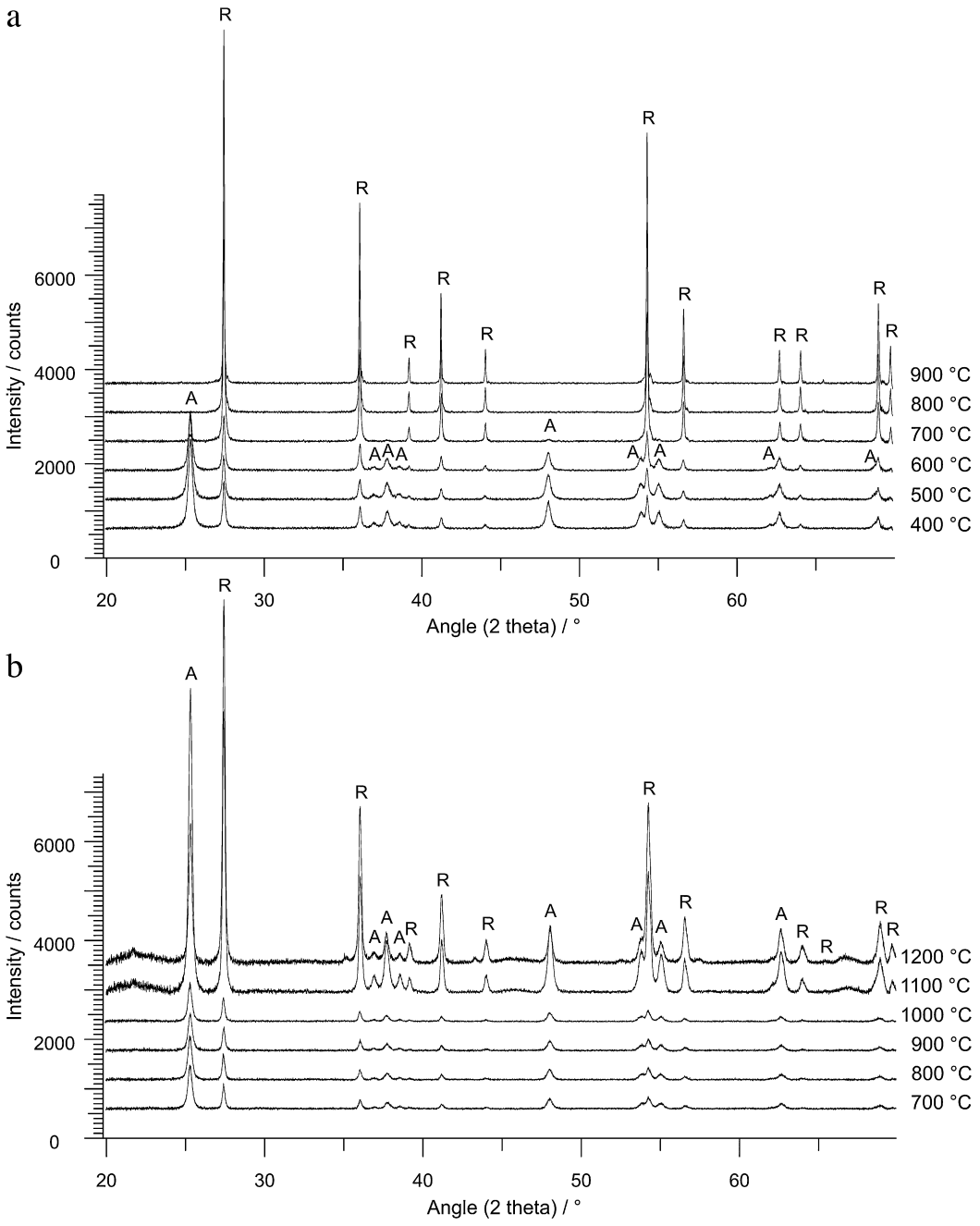

Fig. 1. (a) XRD patterns of anatase powder starting material fired from 400 °C to 900 °C. (b) Stabilised anatase powder S20 fired from 700 °C to 1200 °C. A: anatase; R: rutile.

the methylene blue samples was performed using a Perkin Elmer Lambda 16 photometer at a wavelength of 664 nm.

3. Results and discussion

3.1. Thermal stability of the powders

In order to investigate and optimise the titania thermal stability and titania loading of the powders, the titania fraction was varied between 13 and 98 wt%. Powders with 13, 20, 25, 36, 47, 57, 76, 92, 96 and 98 wt% titania were fired stepwise from 100 to 1300 °C followed by quantitative XRD analysis after every heating step to examine the crystal structure and the thermal stability of the synthesised powders. Compositions with 20 wt% titania (S20) showed the greatest thermal stability, therefore all further experiments were focused on the S20 material. Typical XRD results for the non-stabilised titania starting powder and the thermally stable S20 material as a function of temperature are given in Fig. 1a and b, respectively, with quantitative XRD analysis for S20 given in Fig. 2a. The diffractograms (Fig. 1) showed two main peaks at $2\theta = 25.3^\circ$ and at $2\theta = 27.5^\circ$ which correspond to the anatase (1 0 1) and rutile (1 1 0) lattice planes, respectively. The anatase (A) to rutile (R) phase transition proceeded at temperatures between 500 °C and

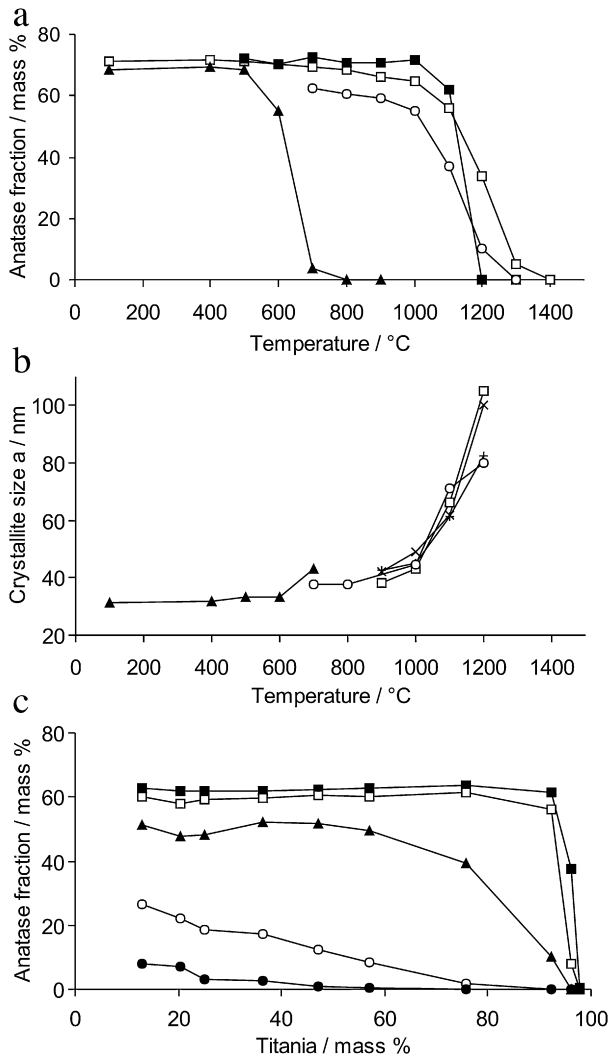

Fig. 2. (a) Thermal stability of stabilised titania and (b) crystallite size dependence on firing temperature: S20 powder (20 wt% titania; □), S20 powder without boehmite (◯), S10 powder (13 wt% titania; +), S70 powder (76 wt% titania; ×), S20 on corundum (■), and non-stabilised anatase starting material (▲). (c) Thermal stability of anatase as a function of the titania fraction in the powder: samples fired at 900 °C (■), 1000 °C (□), 1100 °C (▲), 1200 °C (◯) and 1300 °C (●).

700 °C for the starting material, with the anatase mass fraction decreasing from 68 wt% to 4 wt% in this temperature range. This correlates well to published data for the A–R phase transition temperature for nanocrystalline TiO_2 sol–gel powders.[19] The XRD patterns of the thermally stable material S20 show the A–R phase transformation occurred between 1000 °C and 1200 °C, with the anatase mass fraction decreasing from 70 wt% to 34 wt%, and by 1300 °C the anatase was completely transformed to rutile (Fig. 2a). At 1100 °C an overall increase of the peak intensity was observed due to enhanced anatase crystallinity and crystallite size (Fig. 1b). An increasing crystallite size but constant anatase lattice parameter was observed for all powders with increasing temperature (Fig. 2b). Comparing the A–R transformation temperatures of the anatase starting material and the stabilised anatase S20, a shift of the A–R transition by about 500 °C was found.

Fig. 2c shows the dependence of the anatase fraction on both temperature and wt% titania in the starting mixture. The highest thermal stability was found at lower titania contents (13–36 wt%) and higher silica/boehmite amounts. At 1000 °C higher anatase stability was seen across the broad range of 13–92 wt% titania in the starting mixture. This shows that silicon dioxide and boehmite nanoparticles are effective for improving the thermal stabilisation of the anatase phase compared to the pure titania starting material.

No phases other than anatase and rutile were found in the XRD diffractograms of S20. Silicon dioxide is assumed to remain amorphous, as seen by Okada et al.[38] and any diffraction from boehmite is not visible due to the nanoparticle size producing just a weak and broad XRD signal. Therefore, it can be assumed that the anatase particles were dispersed within an amorphous silicon dioxide and boehmite matrix. Other investigators have found that the A–R transition temperature was affected by the charge and radius of cation and anion additives, grain size, and the atmosphere during heating.[21,38] Quadravalent cations such as Si^{4+} ($r = 0.042$ nm) with a greatly different ionic radius from Ti^{4+} ($r = 0.068$ nm) cannot enter the anatase structure but can surround titania particles and thereby prevent direct contact, grain growth and the A–R phase transformation.[38] The inhibitory effect of alumina itself on the A–R phase transformation has also been observed in previous work.[32,33,39] Considering the case here of using pre-formed titania nanoparticles, one can assume that during dispersion a silica network is formed (from TEOS) which surrounds the titania particles and which at higher temperatures forms an amorphous shell, preventing direct contact and grain growth of the anatase particles and inhibiting the transition to rutile. Improved thermal stability was found when the silica was partially replaced with alumina (Fig. 2a), a feature which was also observed by Yang and Ferreira.[34] The boehmite (γ-AlOOH) which was used for powder synthesis can undergo a phase transition to aluminium oxide (α-Al_2O_3) during heating between 300 °C and 1100 °C.[40]

3.2. FT-IR and UV–vis spectroscopy

FT-IR spectroscopy was performed on the most thermally stable S20 titania powder to investigate the bonding environment of the titania and the silica matrix. The analysis was performed over the wave number range from 4000 to 600 cm^{-1} for powders fired from 100 °C to 1200 °C (Fig. 3a). The absorption band at wave number 1050–1080 cm^{-1} and the shoulder at about 1200 cm^{-1} observed in all spectra could be assigned to asymmetric ν(Si–O–Si) stretching vibrations. Spectra 7 and 9 of powders fired at 1000 °C and 1200 °C, respectively, showed an absorption band at 790 cm^{-1} which was assumed to be from symmetric ν(Si–O–Si) vibrations.[41,42] The absorption band at 1630 cm^{-1} was assigned to hydrated species and the broad band at 2700–3700 cm^{-1} results from vibrations of O–H groups and strongly adsorbed water molecules located on the surface and linked with hydrogen bridges.[42–44] With increasing annealing temperature these absorption bands became very weak because of thermal condensation reactions of the hydroxyl functional groups, loss of water, and a general densification of

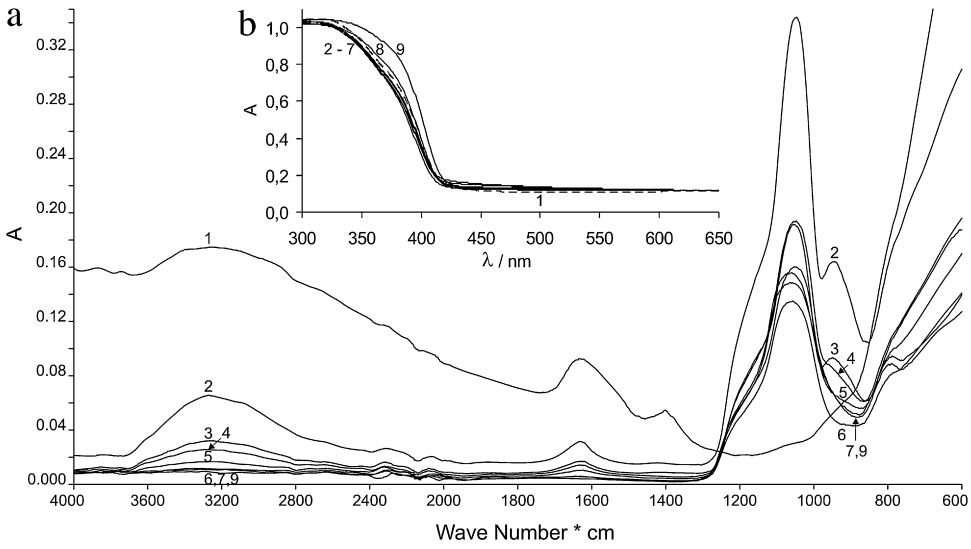

Fig. 3. (a) FT-IR spectroscopy of titania powders: titania starting material (1), S20 fired at 100 °C (2), 200 °C (3), 400 °C (4), 600 °C (5), 800 °C (6), 1000 °C (7), 1100 °C (8), 1200 °C (9). (b) UV–vis spectroscopy of titania powders: titania starting material (1) and stabilised anatase powders S20 (2–9) fired as for FT-IR spectroscopy.

the silicon oxide network. Furthermore, an absorption band at 940–970 cm^{-1} seen at low temperatures in spectra 2–4 (100–400 °C) was found. There is a known absorption band at 910–960 cm^{-1} which is characteristic of Ti–O–Si vibrations, but this could overlap with Si–OH group vibrations at around 980 cm^{-1}.[45] The observed decrease of the absorption band within this region at higher firing temperatures indicates that this is likely to be due to the Si–OH bonds. An absorption band at 1070 cm^{-1} is characteristic for the Si–O–Al vibration,[46] however, this band overlaps with the asymmetric ν(Si–O–Si) stretching vibration and cannot be unambiguously identified. In summary, no Ti–O–Si bonds were found, hence one can assume only weak interactions at the silica–titania interface. The opposite is found when using organotitanium precursors for anatase synthesis, which generates a silica–titania network containing a high amount of Ti–O–Si bonds.[42]

UV–vis reflection spectroscopy between 300 and 650 nm on the S20 powders fired from 100 °C to 1200 °C was performed to investigate the influence of the silicon dioxide and boehmite on the band gap of the titanium dioxide semiconductor. Fig. 3b shows the spectra for the non-stabilised titania starting material (1) and for the stabilised anatase powder S20 (2–9). The spectra showed an onset of absorption at 418 nm for the anatase starting material. The S20 powder fired up to 1000 °C showed only a slight blue shift of the absorption edge to shorter wavelengths with an onset of absorption at 412–415 nm. From these results one can deduce that the titania band gap was barely modified and no penetration of the silica or boehmite into the anatase structure occurred.[47] The anatase powder fired at 1200 °C showed a red shift to longer wavelengths due to the formation of new amorphous phases. Overall the FT-IR and UV–vis results support the model of titania particles encased by an amorphous SiO_2 shell which prevents direct contact and grain growth of the anatase particles and thereby inhibiting the transition to rutile.

3.3. Thermal stability as coatings

A similar series of experiments as for the powders was performed on coatings on crystalline corundum substrates to investigate the influence of an inert substrate on the phase stability of anatase. The corundum substrates were dip-coated with S20 and fired stepwise from 500 °C to 1400 °C. On corundum substrates the diffractograms show an A–R transformation temperature between 1000 °C and 1200 °C (Fig. 4a). The anatase mass fraction decreased from 62 wt% to 0 wt% within this temperature range (Fig. 2a). At 1300 °C mullite formation was found on the substrate. This shows slightly reduced anatase thermal phase stability on corundum compared to S20 powder bulk material.

In order to examine the phase stability of anatase on amorphous glazed substrates similar experiments were performed on three different common lead-free glazes. Due to the lower melting points of the glazes, it was not possible to explore the 1000–1200 °C region at extended times as for the previous samples. Instead, the samples were analysed as a function of holding time when fired at 1080 °C for between 1 and 30 min. A typical example of the XRD patterns produced is shown in Fig. 4b for S20 dip-coated on glaze 3. On the Na–K glaze 1 a complete transformation of anatase to rutile was found after 5 min (Fig. 5). In comparison, the non-stabilised starting material was completely transformed after one minute on the same glaze. Fig. 5 also shows the thermal stability of the stabilised anatase powder S20 and S20 coated on corundum after 30 min at 1080 °C for comparison. On Na–B glaze 2.53 wt% anatase and on glaze 3.61 wt% anatase were found after 5 min at 1080 °C. On glaze 2 the complete A–R phase transformation was found after 15 min and on glaze 3.40 wt% residual anatase was found after 20 min at 1080 °C. It is clear from these results that the thermal stability of S20 stabilised anatase is reduced when coated onto glazed substrates compared to the bulk powder form. In contrast, only a

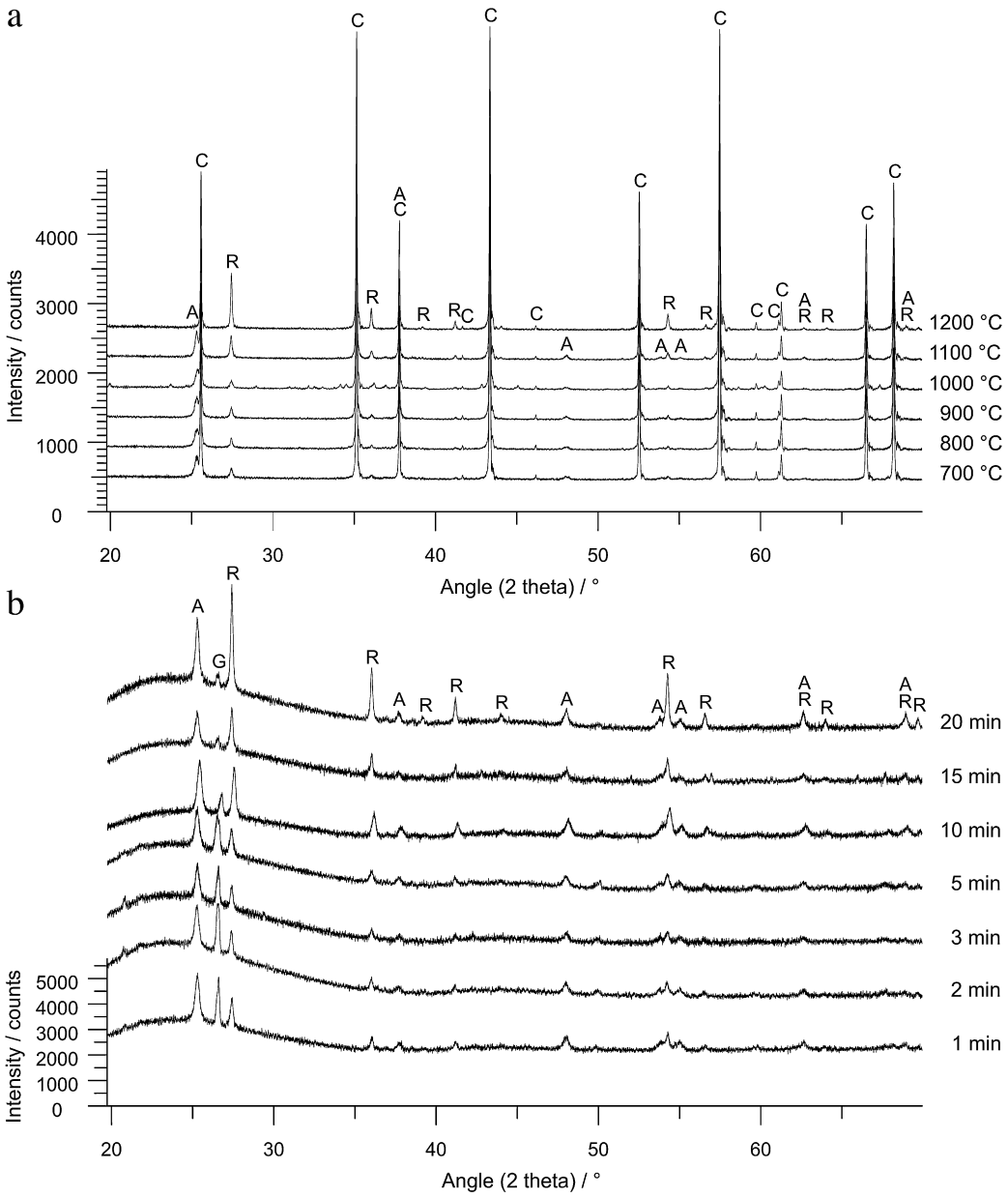

Fig. 4. (a) XRD patterns of stabilised anatase powder S20 coated on corundum and fired from 700 °C to 1200 °C. (b) Stabilised anatase S20 coated on glaze 3 and fired at 1080 °C. A: anatase; R: rutile; C: corundum; G: glaze 3.

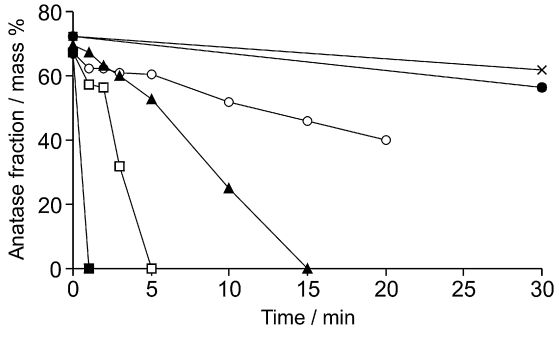

Fig. 5. Thermal stability of anatase S20 coated on three different glazes and on corundum: anatase starting material on glaze 1 (■), S20 on glaze 1 (□), glaze 2 (▲), glaze 3 (◯) and on corundum (●). Stabilised anatase powder S20 (×) fired at 1080 °C.

slight decrease of the thermal stability when coated on the crystalline corundum substrate was seen. In the case of the glazed substrates which contain cations such as Na^+, K^+, Ca^{2+}, Ba^{2+} and B^{3+}, the reduced thermal stability can be understood by assuming the formation of oxygen vacancies by cationic substitution in the TiO_2 at the glaze–titania interface. These vacancies enable the transport of atoms within the anatase structure at high temperature and accelerate the A–R phase transition.[38,48] Na_2O and K_2O for example are major components of glazes 1 and 2 which have been seen to induce an increased A/R phase transition rate in other studies.[25,28] In summary, the thermal stability of anatase coated onto glazes is strongly influenced by the cations present in the glaze and on the ability of the cations to generate oxygen vacancies. Inert and highly crystalline substrates such as corundum do not deliver cations and the titania

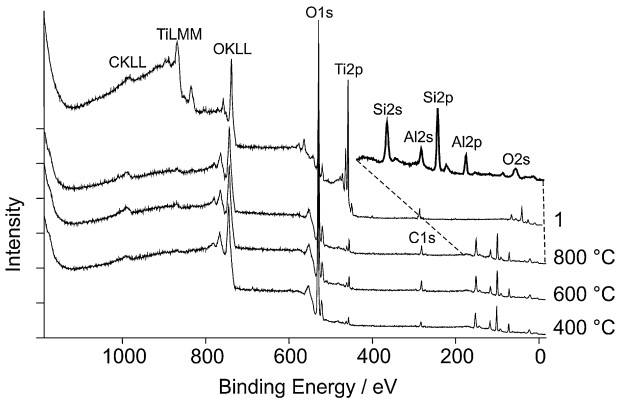

Fig. 6. XPS wide scan spectra of titania coatings: titania starting material (1), S20 fired at 400 °C, 600 °C and 800 °C.

coatings show increased thermal stability. Aside from the direct stabilisation of the titania by addition of silica and alumina, the chemical composition of the glaze substrate plays a key role for the development of photocatalytically active ceramic tiles.

3.4. X-ray photoelectron spectroscopy

Due to the high thermal phase stability of S20 coated on glaze 3, these samples were analysed using X-ray photoelectron spectroscopy (XPS) to investigate the elements present on the coating surface. The analysis was performed on coatings fired between 100 °C and 1000 °C. The spectra showed the following photoelectron peaks: O 1s at a binding energy E_b of 530 eV, Ti2p at E_b of 458 eV, C 1s at E_b of 284 eV, Si 2s at E_b of 153 eV, Al 2s at E_b of 118 eV, Si 2p at E_b of 102 eV, Al 2p at E_b of 73 eV and O 2s at E_b of 23 eV and the CKLL, TiLMM and OKLL auger peaks between 700 and 1000 eV (Fig. 6). The photoelectron peak for O 1s is due to Si–O, Al–O and Ti–O bonds, the peak for Ti 2p is due to the Ti–O bonds, the Si peaks due to Si–O and the Al peaks due to Al–O bonds. The photoelectron peak for C 1s is likely to be due to residual carbon produced by incomplete pyrolysis of alkoxide precursors and ethanol. The ratios of the elements on the surface varied only slightly when increasing the firing temperature. A molar ratio of 67/31/2 Si/Al/Ti was found on the sample fired for 800 °C. Based on this XPS analysis one could deduce that only a minor amount of titania is present within the upper few nanometers of the coating surface. Considering the use of pre-formed titania nanoparticles and a polymerisable organosilicon precursor, this result can be explained by assuming that an amorphous silica shell encases the titania particles which leads to less TiO_2 accessible to XPS and more SiO_2 on the surface. Additionally a high deflection and partial absorption of the TiO_2 electrons by SiO_2 on their way to the detector lower the XPS measured titania content.

3.5. EDS elemental mapping

To investigate the distribution of the S20 particles within the coatings, an element map was generated using SEM-EDS (Fig. 7). An even dispersion of titanium, silicon and aluminium is shown. The dip-coating process has therefore maintained a homogeneous distribution of the particles on the glaze surface. Considering that the thermal stability of anatase depends on good dispersion within the silica matrix to prevent direct contact

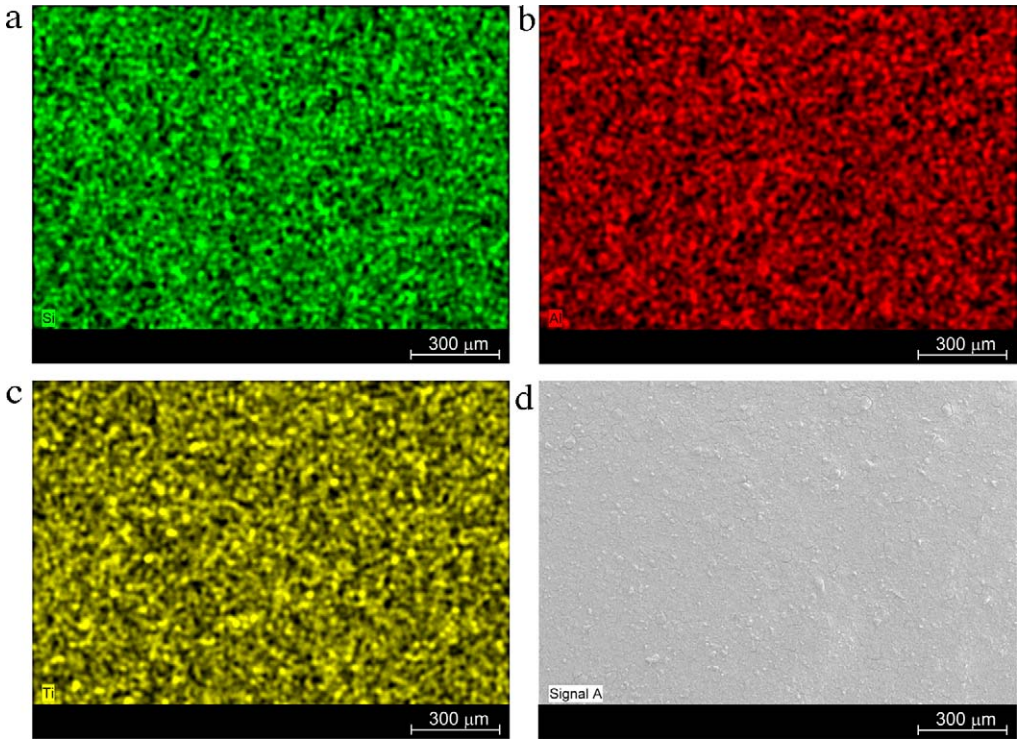

Fig. 7. SEM-EDS analysis of stabilised anatase S20 dip-coated on glaze 3. Mapping of silicon (a), aluminium (b) and titanium (c). SEM of stabilised anatase S20 dip-coated on glaze 3 and dried at 100 °C (d).

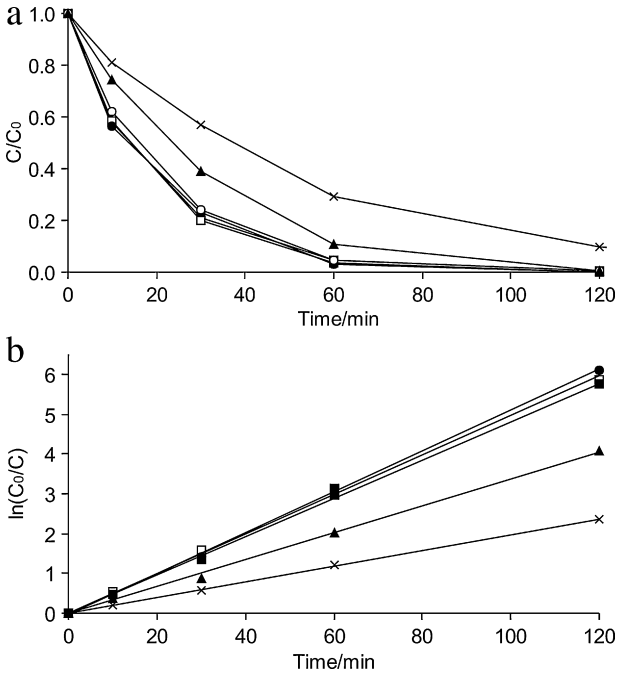

Fig. 8. Photocatalytic activity of stabilised anatase S20 coated on corundum and fired at 800 °C (□), 900 °C (■), 1000 °C (●), 1100 °C (◯) and 1200 °C (▲) and the reference photocatalysis without titania (×). Normalised (a) and linearised degradation curves (b).

between anatase particles[38] a random dispersion of the titania is important for high thermal stability. On the other hand, with respect to the correlation between high specific surface area and catalytic activity, an even distribution of the titania is also important for achieving highly photocatalytically active surfaces.

3.6. Photocatalytic activity of the coatings

The photocatalytic activity of the stabilised S20 material was investigated using methylene blue (MB) in water as a model organic substance for photocatalytic degradation.[49] The photocatalytic activity for S20 on corundum was determined by UV–vis spectroscopy for different firing temperatures between 800 °C and 1200 °C. Fig. 8 shows the normalised degradation curves (C/C_0) up to 120 min, which were linearized via $\ln(C_0/C)$ log transformation according to the first-order Langmuir-Hinshelwood kinetic equation.[49–52] Control experiments in the absence of titania coatings showed that MB was partially degraded by photolysis. As a result Fig. 8 shows a similar photocatalytic activity for coatings prepared on corundum between 800 °C and 1100 °C. For coatings on corundum fired at 1200 °C a reduced photocatalytic activity was found due to the A–R phase transformation that occurred between 1100 °C and 1200 °C. Hence the firing temperature is an important parameter that affects the photocatalytic activity of the material, especially considering that the firing temperature controls both the titania morphology and the A–R transition rate, respectively.[17] Therefore 1100 °C is the highest possible firing temperature for titania on corundum substrates to prevent the A–R phase transformation and conserve the anatase structure and a high photocatalytic activity.

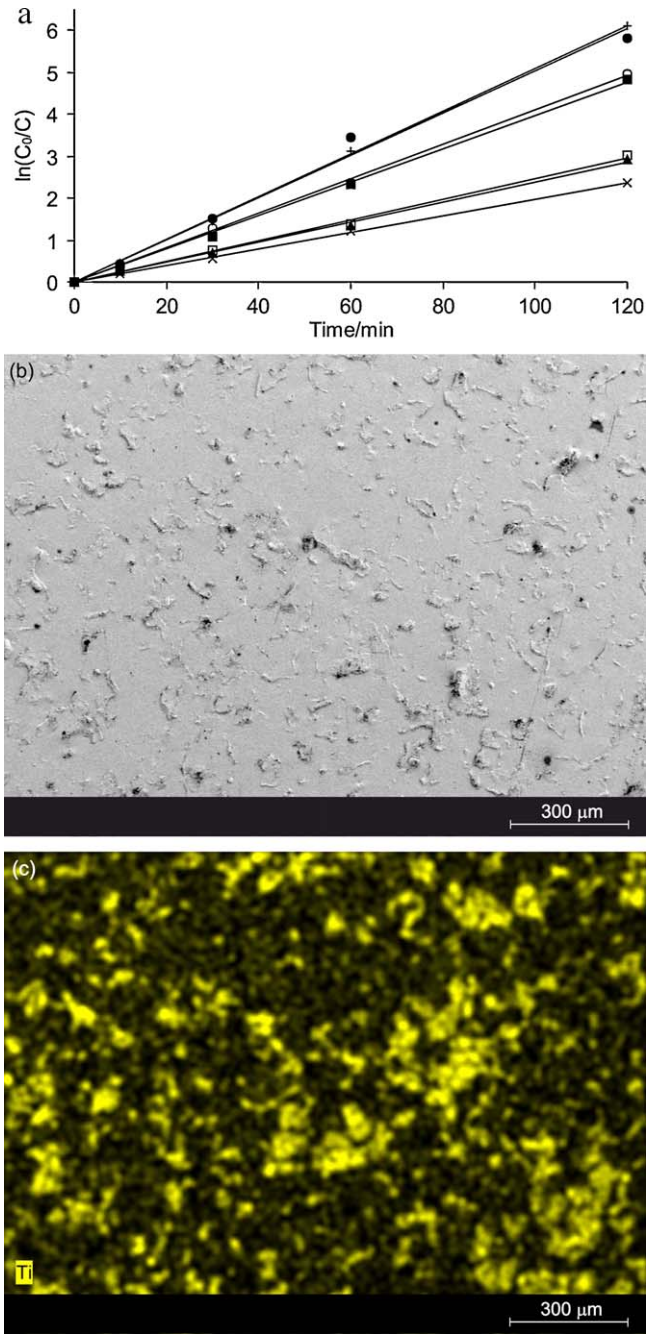

Fig. 9. (a) Photocatalytic activity of stabilised anatase powder S20 dip-coated on glaze 1 (◯), 2 (●), 3 (■) and corundum (+) and fired at 1080 °C, compared with commercial available titania coatings on glass (□), ceramic tiles (▲) and the reference photolysis activity without titania (×). SEM (b) and EDS (c) analysis of S20 on glaze 3 fired at 1100 °C.

The photocatalytic activity was also investigated on the three different glazed substrates (Fig. 9a). Each glaze was applied on the substrate, fired, then the stabilised anatase S20 was applied by dip-coating in a separate step. After drying the coating was fired at 1080 °C for 1, 2, 3 and 5 min. The firing time at the melting point of the glaze is an important factor for incorporating and fixing the titania coating within the glaze to obtain

abrasion-resistant surfaces. SEM analysis (Fig. 9b) shows the incorporation of the S20 titania within the coating after firing, however titania was found on the surface by EDS mapping (Fig. 9c). The photocatalytic activity of the coatings on glazes 1–3 were compared to the activity on corundum and to two commercially available titania coatings on glass and on ceramic tiles. On corundum and on glaze 2 a higher photocatalytic activity was found compared to all other samples. Based on this result one can deduce that the substrate composition not only affects the anatase phase stability (Fig. 5), but also the general photocatalytic activity of the stabilised anatase S20 material. At high temperature the corundum substrates are more inert than the glazed substrates because no diffusion of cations at the substrate–titania interface is possible. The glazes however contain a variety of cations which are more mobile (e.g. Na^+, K^+) and which can penetrate the silica–alumina–titania structure at high temperature and reduce the photocatalytic activity. This dependency of the photocatalytic activity on the chemical composition of the substrate was also seen by Yao et al.[53] when comparing glass, glazed ceramic, ceramic and metals, and Fernández et al.[54] who found different photocatalytic activities on quartz, steel and glass. It is assumed that cations present in the substrate penetrate the titania structure and reduce the photocatalytic activity by recombination of the electrons (e^-) and the electron holes (h^+).[53–56] Nevertheless, the titania surfaces developed in this work showed a higher photocatalytic activity compared to commercially available glasses and ceramic tiles (Fig. 9).

4. Conclusions

Pre-formed titania nanoparticle dispersions can be made thermally stable up to 1200 °C by the addition of amorphous silica and boehmite nanoparticles. The thermal stabilisation is improved by partially replacing the silica with a source of alumina. The thermal stability of the stabilised anatase dip-coated onto substrates was generally lower than the stabilised bulk powder, and the extent of stability reduction depended on the chemical composition of the substrate material. Glazed surfaces contained the even distribution of titania particles and the photocatalytic activity on such surfaces depended on the chemical composition of the glazes. Therefore, in addition to the elements used to directly stabilise the titania, the chemical composition of the substrate plays a key role in developing thermally stable and photocatalytically active ceramic tiles at temperatures above 1000 °C. In light of (a) the absence of crystalline silica seen in the XRD analysis, (b) the absence of Ti–O–Si interactions seen in FT-IR and UV–vis spectroscopy which showed only a slight modification of the electronic structure, and (c) the minor amounts of titania on the surface seen in XPS measurements, we propose a model similar to that of Okada et al.[38] where the titania particles become surrounded by a network of silica and the boehmite nanoparticles. At higher temperatures densification encases the titania particles with an amorphous and porous silica and alumina shell, which enables photocatalytic activity but prevents direct contact and grain growth of the titania particles and hence the anatase to rutile phase transition.

Acknowledgements

We thank Dr. K. Dänhardt for XPS and P. Bühlmann for SEM-EDS measurements and Dr. M. Terner for constructive discussions.

References

1. Fujishima A, Zhang X, Tryk DA. TiO_2 photocatalysis and related surface phenomena. *Surf Sci Rep* 2008;**63**:515–82.
2. Chen X, Mao SS. Titanium dioxide nanomaterials: synthesis, properties, modifications, and applications. *Chem Rev* 2007;**107**:2891–959.
3. Thompson TL, Yates JT. Surface science studies of the photoactivation of TiO_2—new photochemical processes. *Chem Rev* 2006;**106**:4428–53.
4. Mills A, Le Hunte S. An overview of semiconductor photocatalysis. *J Photochem Photobiol A* 1997;**108**:1–35.
5. Hoffmann MR, Martin ST, Choi W, Bahnemann W. Environmental applications of semiconductor photocatalysis. *Chem Rev* 1995;**95**:69–96.
6. Agrios AG, Gray KA. Beyond photocatalytic environmental remediation: novel TiO_2 materials and applications. In: Grassian VH, editor. *Environmental Catalysis*. Boca Raton: Taylor and Francis Group; 2005. p. 369–90.
7. Kikuchi Y, Sunada K, Iyoda T, Hashimoto K, Fujishima A. Photocatalytic bactericidal effect of TiO_2 thin films: dynamic view of the active oxygen species responsible for the effect. *J Photochem Photobiol A* 1997;**106**:51–6.
8. Sunada K, Watanabe T, Hashimoto K. Studies on photokilling of bacteria on TiO_2 thin film. *J Photochem Photobiol A* 2003;**156**:227–33.
9. Tsuang YH, Sun JS, Huang YC, Lu CH, Hong-Shong Chang W, Wang CC. Studies of photokilling bacteria using titanium dioxide nanoparticles. *Artif Organs* 2008;**32**:167–74.
10. Cho M, Chung H, Choi W, Yoon J. Different inactivation behaviors of MS-2 phage and *Escherichia coli* in TiO_2 photocatalytic disinfection. *Appl Environ Microbiol* 2005;**71**:270–5.
11. Zan L, Fa W, Peng T, Gong Z. Photocatalysis effect of nanometer TiO_2 and TiO_2-coated ceramic plate on hepatitis B virus. *J Photochem Photobiol B* 2007;**86**:165–9.
12. Xu J, Sun Y, Huang J, Chen C, Liu G, Jiang Y, et al. Photokilling cancer cells using highly cell-specific antibody-TiO_2 bioconjugates and electroporation. *Bioelectrochemistry* 2007;**71**:217–22.
13. Rozhkova EA, Ulasov I, Lai B, Dimitrijevic MN, Lesniak MS, Rajh T. A high-performance nanobio photocatalyst for targeted brain cancer therapy. *Nano Lett* 2009;**9**:3337–42.
14. Hund-Rinke K, Simon M. Ecotoxic effect of photocatalytically active nanoparticles (TiO_2) on algae and daphnids. *Environ Sci Pollut Res Int* 2006;**13**:1–8.
15. Zan L, Peng ZH, Xia YL, Huang L. Novel route to prepare TiO_2-coated ceramic and its photocatalytic function. *J Mater Sci* 2004;**39**:761–3.
16. Banfield JF, Gribb AA. Particle size effects on transformation kinetics and phase stability in nanocrystalline TiO_2. *Am Mineral* 1997;**82**:717–28.
17. Banfield JF, Zhang H. New kinetic model for the nanocrystalline anatase-to-rutile transformation revealing rate dependence on number of particles. *Am Mineral* 1999;**84**:528–35.
18. Madras G, McCoy BJ, Navrotsky A. Kinetic model for TiO_2 polymorphic transformation from anatase to rutile. *J Am Ceram Soc* 2007;**90**:250–5.
19. Stir M, Nicula R, Burkel E. Pressure–temperature phase diagrams of pure and Ag-doped nanocrystalline TiO_2 photocatalysts. *J Eur Ceram Soc* 2006;**26**:1547–53.
20. Rego E, Marto J, São Marcos P, Labrincha JA. Decolouration of Orange II solutions by TiO_2 and ZnO active layers screen-printed on ceramic tiles under sunlight irradiation. *Appl Catal A* 2009;**355**:109–14.
21. São Marcos P, Marto J, Trindade T, Labrincha JA. Screen-printing of TiO_2 photocatalytic layers on glazed ceramic tiles. *J Photochem Photobiol A* 2008;**197**:125–31.

22. Bondioli F, Taurino R, Ferrari AM. Functionalization of ceramic tile surface by sol–gel technique. *J Colloid Interface Sci* 2009;**334**:195–201.
23. Yoo SJ, Lee SI, Kwak DH, Kim KG, Hwang KJ, Lee JW, et al. Photocatalytic degradation of methylene blue and acetaldehyde by TiO_2/glaze coated porous red clay tile. *Korean J Chem Eng* 2008;**25**:1232–8.
24. Gennari FC, Pasquevich DM. Enhancing effect of iron chlorides on the anatase–rutile transition in titanium dioxide. *J Am Ceram Soc* 1999;**82**:1915–21.
25. Gennari FC, Pasquevich DM. Kinetics of the anatase–rutile transformation in TiO_2 in the presence of Fe_2O_3. *J Mater Sci* 1998;**33**:1571–8.
26. Iida Y, Ozaki S. Grain growth and phase transformation of titanium oxide during calcination. *J Am Ceram Soc* 1961;**44**:120–7.
27. Mac Kenzie KJD. Calcination of titania: V. Kinetics and mechanisms of the anatase–rutile transformation on the presence of additives. *Trans J Br Ceram Soc* 1975;**74**:77–84.
28. Grzmil B, Kic B, Rabe M. Inhibition of the anatase–rutile phase transformation with addition of K_2O, P_2O_5 and Li_2O. *Chem Pap* 2004;**58**:410–4.
29. Francisco MSP, Mastelaro VR. Inhibition of the anatase–rutile phase transformation with addition of CeO_2 to CuO–TiO_2 system: Raman spectroscopy, X-ray diffraction and textural studies. *Chem Mater* 2002;**14**:2514–8.
30. De Farias RF, Airoldi C. A study about the stabilization of anatase phase at high temperatures on sol–gel cerium and copper doped titania and titania–silica powders. *J Non-Cryst Solids* 2005;**351**:84–8.
31. Setiawati E, Kawano K. Stabilization of anatase phase in the rare earth; Eu and Sm ion doped nanoparticle TiO_2. *J Alloys Compd* 2008;**451**:293–6.
32. Ding X, Liu L, Ma X, Qi Z, He Y. The influence of alumina dopant on the structural transformation of gel-derived nanometer titania powders. *J Mater Sci Lett* 1994;**13**:462–4.
33. Yang J, Huang YX, Ferreira JMF. Inhibitory effect of alumina additive on the titania phase transformation of a sol–gel-derived powder. *J Mater Sci Lett* 1997;**16**:1933–5.
34. Yang J, Ferreira JMF. Inhibitory effect of the Al_2O_3–SiO_2 mixed additives on the anatase–rutile phase transformations. *Mater Lett* 1998;**36**:320–4.
35. Baiju KV, Periyat P, Pillai K, Mukundan P, Warrier KGK, Wunderlich W. Enhanced photoactivity and anatase thermal stability of silica–alumina mixed oxide additives on sol–gel nanocrystalline titania. *Mater Lett* 2007;**61**:1751–5.
36. Periyat P, Baiju KV, Mukundan P, Pillai PK, Warrier KGK. High temperature stable mesoporous anatase TiO_2 photocatalyst achieved by silica addition. *Appl Catal A* 2008;**349**:13–9.
37. Taut T, Kleeberg R, Bergmann J. The new Seifert Rietveld program BGMN and its application to quantitative phase analyse. *Mater Struct* 1998;**5**:57–64.
38. Okada K, Yamamoto N, Kameshima Y, Yasumori A. Effect of silica additive on the anatase-to-rutile phase transition. *J Am Ceram Soc* 2001;**84**:1591–6.
39. Rajesh S, Pillai SC, Hareesh US, Mukundan P, Warrier KGK. Synthesis of thermally stable, high surface area anatase–alumina mixed oxides. *Mater Lett* 2000;**43**:286–90.
40. Levin I, Brandon D. Metastable alumina polymorphs: crystal structures and transition sequences. *J Am Ceram Soc* 1998;**81**:1995–2010.
41. Dutoit DCM, Schneider M, Baiker A. Titania–silica mixed oxides: I. Influence of sol–gel and drying conditions on structural properties. *J Catal* 1995;**153**:165–76.
42. Müller CA, Maciejewski M, Mallat T, Baiker A. Organically modified titania–silica aerogels for the epoxidation of olefins and allylic alcohols. *J Catal* 1999;**184**:280–93.
43. Reddy BM, Reddy KG, Rao KN, Ganesh I, Ferreira JMF. Characterization and photocatalytic activity of TiO_2–M_xO_y ($M_xO_y = SiO_2$, Al_2O_3, and ZrO_2) mixed oxides synthesized by microwave-induced solution combustion technique. *J Mater Sci* 2009;**44**:4874–82.
44. Gun'ko VM, Blitz JP, Gude K, Zarko VI, Goncharuk EV, Nychiporuk YM, et al. Surface structure and properties of mixed fumed oxides. *J Colloid Interface Sci* 2007;**314**:119–30.
45. Beck C, Mallat T, Bürgi T, Baiker A. Nature of active sites in sol–gel TiO_2–SiO_2 epoxidation catalysts. *J Catal* 2001;**204**:428–39.
46. Oréfice RL, Vasconcelos WL. Sol–gel transition and structural evolution on multicomponent gels derived from the alumina–silica system. *J Sol–Gel Sci Technol* 1997;**9**:239–49.
47. Tobaldi DM, Tucci A, Škapin AS, Esposito L. Effects of SiO_2 addition on TiO_2 crystal structure and photocatalytic activity. *J Eur Ceram Soc* 2010;**30**:2481–90.
48. Jean J, Lin S. Kinetics and mechanism of anatase-to-rutile phase transformation in the presence of borosilicate glass. *J Mater Res* 1999;**14**:2922–8.
49. Houas A, Lachheb H, Ksibi M, Elaloui E, Guillard C, Herrmann JM. Photocatalytic degradation pathway of methylene blue in water. *Appl Catal B* 2001;**31**:145–57.
50. Fox MA, Dulay MT. Heterogenous photocatalysis. *Chem Rev* 1993;**93**:341–57.
51. McMurray TA, Byrne JA, Dunlop PSM, Winkelmann JGM, Eggins BR, McAdams ET. Intrinsic kinetics of photocatalytic oxidation of formic and oxalic acid on immobilized TiO_2 films. *Appl Catal A* 2004;**262**:105–10.
52. Konstantinou IK, Albanis TA. TiO_2-assisted photocatalytic degradation of azo dyes in aqueous solution: kinetic and mechanistic investigations: a review. *Appl Catal B* 2004;**49**:1–14.
53. Yao M, Chen J, Zhao C, Chen Y. Photocatalytic activities of Ion doped TiO_2 thin films when prepared on different substrates. *Thin Solid Films* 2009;**517**:5994–9.
54. Fernández A, Lassaletta G, Jiménez VM, Justo A, González-Elipe AR, Herrmann JM, et al. Preparation and characterization of TiO_2 photocatalysts supported on various rigid supports (glass, quartz and stainless steel). Comparative studies of photocatalytic activity in water purification. *Appl Catal B* 1995;**7**:49–63.
55. Tomaszewski H, Eufinger K, Poelman H, Poelman D, De Gryse R, Smet PF, et al. Effect of substrate sodium content on crystallization and photocatalytic activity of TiO2 films prepared by DC magnetron sputtering. *Int J Photoenergy* 2007.
56. Eufinger K, Janssen EN, Poelman H, Poelman D, De Gryse R, Marin GB. The effect of argon pressure on the structural and photocatalytic characteristics of TiO_2 thin films deposited by d.c. magnetron sputtering. *Thin Solid Films* 2006;**515**:425–9.